Comparison of quantitative Y-90 SPECT and non-time-of-flight PET imaging in post-therapy radioembolization of liver cancer

Jianting Yue
Russell H. Morgan Department of Radiology and Radiological Science, Johns Hopkins University, Baltimore, Maryland 21287

Thibault Mauxion
Biocompatibles UK Ltd, A BTG Group Company, Camberley, GU15 3YL, United Kingdom

Diane K. Reyes and Martin A. Lodge
Russell H. Morgan Department of Radiology and Radiological Science, Johns Hopkins University, Baltimore, Maryland 21287

Robert F. Hobbs
Russell H. Morgan Department of Radiology and Radiological Science, Johns Hopkins University, Baltimore, Maryland 21287 and Department of Radiation Oncology, Johns Hopkins University, Baltimore, Maryland 21287

Xing Rong
Siemens Medical Solutions USA Inc., Hoffman Estates, Illinois 60192

Yinfeng Dong
Russell H. Morgan Department of Radiology and Radiological Science, Johns Hopkins University, Baltimore, Maryland 21287

Joseph M. Herman
Department of Radiation Oncology, Johns Hopkins University, Baltimore, Maryland 21287

Richard L. Wahl
Department of Diagnostic Radiology, Mallinckrodt Institute of Radiology, Washington University School of Medicine, St. Louis, Missouri 06310

Jean-François H. Geschwind
Department of Radiology, Yale University School of Medicine, New Haven, Connecticut 06520

Eric C. Frey[a)]
Russell H. Morgan Department of Radiology and Radiological Science, Johns Hopkins University, Baltimore, Maryland 21287

(Received 3 May 2016; revised 11 July 2016; accepted for publication 25 August 2016; published 30 September 2016)

Purpose: Radioembolization with yttrium-90 microspheres may be optimized with patient-specific pretherapy treatment planning. Dose verification and validation of treatment planning methods require quantitative imaging of the post-therapy distribution of yttrium-90 (Y-90). Methods for quantitative imaging of Y-90 using both bremsstrahlung SPECT and PET have previously been described. The purpose of this study was to compare the two modalities quantitatively in humans.
Methods: Calibration correction factors for both quantitative Y-90 bremsstrahlung SPECT and a non-time-of-flight PET system without compensation for prompt coincidences were developed by imaging three phantoms. The consistency of these calibration correction factors for the different phantoms was evaluated. Post-therapy images from both modalities were obtained from 15 patients with hepatocellular carcinoma who underwent hepatic radioembolization using Y-90 glass microspheres. Quantitative SPECT and PET images were rigidly registered and the total liver activities and activity distributions estimated for each modality were compared. The activity distributions were compared using profiles, voxel-by-voxel correlation and Bland–Altman analyses, and activity-volume histograms.
Results: The mean ± standard deviation of difference in the total activity in the liver between the two modalities was 0% ± 9% (range −21%–18%). Voxel-by-voxel comparisons showed a good agreement in regions corresponding roughly to treated tumor and treated normal liver; the agreement was poorer in regions with low or no expected activity, where PET appeared to overestimate the activity. The correlation coefficients between intrahepatic voxel pairs for the two modalities ranged from 0.86 to 0.94. Cumulative activity volume histograms were in good agreement.

Conclusions: These data indicate that, with appropriate reconstruction methods and measured calibration correction factors, either Y-90 SPECT/CT or Y-90 PET/CT can be used for quantitative post-therapy monitoring of Y-90 activity distribution following hepatic radioembolization. [http://dx.doi.org/10.1118/1.4962472]

Key words: yittrium-90 bremsstrahlung, quantitative SPECT, yttrium-90 PET, selective internal radiation therapy, radioembolization

1. INTRODUCTION

Radioembolization (RE), also referred to as selective internal radiation therapy (SIRT) or microsphere brachytherapy, of liver cancer involves delivery of Y-90 microspheres via a catheter placed in the right, left, or a subselective hepatic artery. Optimal therapeutic planning would require knowledge of the absorbed dose (AD) to tumors and normal liver per unit administered activity (AA). Wide variation in the dose to tumors and normal liver results from differences in hemodynamics and tumor burden among patients.[1,2] Dosimetry estimates used in clinical practice are often quite simple and are designed to prevent toxicity to nontumor involved liver.[1]

One approach to pretherapy dosimetry is the use of pretherapy imaging using Tc-99m macroaggregated albumin (MAA) delivered intra-arterially. In conventional therapy, Tc-99m MAA planar imaging is used to measure shunting to the lungs as well as to trace unintended delivery of particles to other extra-hepatic structures.[3,4] However, quantitative SPECT (QSPECT) methods can provide an estimate of the Tc-99m activity distribution, which could serve as a surrogate for the Y-90 activity distribution from an RE procedure.[5–7]

The range of particle sizes (diameters) is different for MAA (0–150 μm) than for the Y-90 microspheres (20–60 μm, depending on the product). As a result, it is highly desirable to be able to image the Y-90 activity distribution after a therapeutic administration in order to verify the delivered dose to tumors and normal organs and thus to validate planning methods.[8]

The Y-90 activity distribution cannot be imaged quantitatively with conventional QSPECT methods as it decays without emission of gamma photos suitable for imaging. An alternative is to image the bremsstrahlung photons.[1] QSPECT of these photons is difficult due to the wide and continuous energy spectrum, but several recent papers have described methods and acquisition parameters for Y-90 QSPECT.[9–13]

An alternative is to use PET imaging, which takes advantage of the small fraction (3.186×10^{-5}) of the Y-90 decays that result in the emission of positrons. The Y-90 activity image is quantified by taking into account the branching ratio for this decay mode, though quantification is complicated by high energy bremsstrahlung emissions and the minute positron fraction.[14–16]

There have been several recent papers evaluating methods for quantitative Y-90 imaging.[12,13,17] A recent multicenter phantom study evaluated the performance of a variety of PET systems with and without time-of-flight (ToF) capability.[17] It was found that ToF systems provided higher accuracy, with an average accuracy for estimating the background concentration of 1%–5% (range +4% to −9%) for scanners from the three major vendors with ToF and +2% to −9% (range +9% to −29%) for non-ToF systems. A phantom study comparison of ToF PET to bremsstrahlung SPECT using standard manufacturer-provided reconstruction, attenuation compensation, and resolution recovery showed substantially higher accuracy for the PET, with an error in activity concentration in a 37 mm sphere of 11% for ToF PET and 58% for SPECT.[13]

In this clinical study, we developed and validated calibration methods and compared non-ToF Y-90 PET and a multienergy-range (MER) Y-90 quantitative bremsstrahlung SPECT (QBSPECT) method[11] quantitatively using patient studies. Post-therapy imaging of patients undergoing RE using Y-90 glass microspheres was acquired using both modalities. The modalities were compared in terms of differences in the total activity in the liver and measures of agreement of the activity distribution in the liver.

2. MATERIALS AND METHODS

2.A. SPECT and PET calibration experiments

The quantitative accuracy of SPECT reconstruction largely depends on the accuracy of the model of the image formation process used in the reconstruction algorithm. The MER method uses Monte Carlo simulation to estimate the geometric sensitivity, collimator-detector response (CDR) tables, and scatter kernels used in the quantitative reconstructions.[11] These simulations depend on *a priori* knowledge of various collimator and detector parameters.[18] Many of these parameters could not be measured directly, and manufacturer provided values were thus used. However, uncertainties in the values of these parameters and approximations in the MER method potentially limit the quantitative accuracy of the reconstructions.[11,19] Here we used calibration correction factors (CCFs), described in detail below, to account for these effects.

Quantitative Y-90 PET on the scanner used in this work also requires calibration to be quantitatively accurate, as will be shown below.

For both modalities, the CCF can, in principle, depend on the object imaged. As a result, we measured the CCF using three phantoms more representative of humans (Table I) than the rod phantoms used previously.[11]

TABLE I. Phantom shapes and sizes.

Phantom	Object dimensions (cm)	Volume[a] (ml)	Activity (MBq)[b]
Large uniform cylinder	Length: 20		D670: 441
	Diameter: 20.6	5635	Symbia: 338
			DRX: 525
Small uniform cylinder	Length: 18.6		D670: 278
	Diameter: 4.5	291	Symbia: -
			DRX: 346
Sphere in cold	Major axis: 31.2		Discovery 670: 545
elliptical phantom	Minor axis: 25.0	89.6	Symbia: 321
	Length: 18.6		Discovery RX: 416
	Sphere diameter: 5.5		

[a]Volume of the compartment containing the activity.
[b]The activity inside the phantom at the scan time for GE Discovery 670 SPECT/CT (D670), Siemens Symbia (Symbia) SPECT/CT, and GE Discovery RX (DRX) PET/CT systems.

2.A.1. Calculation of calibration correction factors

Both QBSPECT and PET give quantitative images with voxel values in units of activity concentration. The CCF is given by the true activity in the volume-of-interest (VOI) divided by the total activity estimated from the quantitative image in some VOI before multiplication by the CCF.

For QBSPECT, we defined VOIs in the quantified reconstructed images based on the registered CT images. To partly offset partial volume effects in the QBSPECT images, the VOI boundary was drawn about 3 pixels outside the physical boundary. The QBSPECT method provided voxel values in units of decays per voxel, so dividing by the total imaging time gave an image in units of activity per voxel.

To investigate the need for a CCF with PET, we scanned the same phantoms using the protocol and scanner described below. The method used to calculate the CCF relied on activity concentration rather than total activity. For PET, VOIs were drawn at a distance of 2–3 times the full-width-half-maximum (FWHM) inside the CT boundary to avoid partial volume and edge effects. The average activity concentration inside this VOI was then multiplied by the volume of the whole compartment to obtain the total activity. This method was used for Y-90 PET because there was nonzero activity in the reconstructed images in regions outside the phantom or where there was no activity (discussed below). The CCF for PET was obtained by dividing the activity placed in the compartment by the measured total activity.

2.A.2. Activity calibration measurement

The computations for the CCF required the "true" activity in the phantom. This was measured using a Capintec model 55tR activity meter, calibrated within a day of each measurement using Cs-137, Ba-133, and Co-57 sources with activities traceable to NIST standards using manufacturer recommended procedures. Y-90 activity was measured in 3 ml plastic syringes for all the experiments. The activity in the syringe before and after injecting the solution into the phantom was measured using the dose calibrator setting recommended for a syringe as in Ref. 20.

2.A.3. SPECT/CT image acquisition and reconstruction

SPECT/CT data were acquired using a GE Discovery 670 and a Siemens Symbia T16 SPECT/CT system. For both, we used a 128×128 projection matrix and bin sizes of 0.442 and 0.480 cm for the GE and Siemens systems, respectively. Both systems had 9.525-mm thick crystals. An HEGP collimator was used in both cases, though the design parameters were different. The acquisition energy window was 100–300 keV. Scans were acquired at 120 views over a 360° angular range, with a 45 s acquisition duration at each view.

Image reconstructions were performed using the OS-EM algorithm and the MER method.[11] In this method, the modeling of scatter, attenuation, and the CDR was performed in multiple energy ranges to allow modeling the energy dependence of these factors. Attenuation modeling took into account beam hardening via the use of effective attenuation coefficients in each energy range. Scatter and downscatter were modeled using the effective source scatter estimation (ESSE) method.[21] We investigated 5, 10, 40, and 100 iterations, with 12 subsets per iteration, in order to study the effect of the iteration number on activity estimates. The voxels in the reconstructed images had a side length equal to the projection bin size for both systems. Images were smoothed with a 7 mm FWHM Gaussian filter to control image noise. Reconstructed patient images were multiplied by the CCF to produce the QSPECT image.

2.A.4. PET/CT image acquisition and reconstruction

A non-ToF LYSO-based GE Discovery RX PET/CT system was used for Y-90 PET. Its axial field of view (FOV) is 15.3 cm. The scans were performed in 3D mode using one bed position and an acquisition duration of 30 min for both phantom and patient studies.

The transaxial reconstructed voxel size was 0.47 cm, and the slice thickness was 0.33 cm. The images were reconstructed using the vendor-provided OS-EM algorithm, using two iterations with 21 subsets per iteration. A postreconstruction 7 mm FWHM Gaussian filter was applied. CT attenuation, random corrections based on single rates, single scatter correction, and dead time corrections were included in the reconstruction process. The positron fraction for Y-90 used in the reconstruction was 3.186×10^{-5}. Reconstructed patient images were divided by the CCF for PET to produce the image used for quantitative comparisons.

2.B. Patient study

2.B.1. Patient demographics

Patient data were acquired as part of two prospective studies approved by the Johns Hopkins Institutional Review Board. The first was a pilot study to perform initial validation

TABLE II. Patient demographics.

Patient	Gender	Age	Disease	SPECT/CT scanner	Scan gap[a] (h)	Lobes treated[b]	AA[c] (MBq)	LSF[d] (%)	Treated volume (ml)
1	M	78	mCRC[e]	GE Discovery	2.7	R	3709	2.86	748
2	M	49	mCRC	GE Discovery	1.6	L	1823	4.5	1438
3	M	53	mCRC	Siemens Symbia	−0.8	R	4155	8.7	1445
4	F	51	mPNET[f]	Siemens Symbia	2.4	L[g]	3100	4.1	1706
5	M	65	HCC[h]	GE discovery	1.4	R	2324	22.0	1708
6	M	58	HCC	Siemens Symbia	2.3	R	847	23.5	389
7	M	63	HCC	Siemens Symbia	2.3	R	3382	1.6	1470
8	M	56	HCC	GE discovery	3.5	L	1099	6.8	397
9	F	56	HCC	Siemens Symbia	−0.4	R	5287	5.0	2012
10	M	43	HCC	GE Discovery	−0.9	R	4780	7.1	1939
11	M	62	HCC	GE Discovery	−1.3	R	3300	2.4	1322
12	F	80	HCC	Siemens Symbia	−0.9	R	1598	1.2	681
13	M	80	HCC	Siemens Symbia	1.4	R	1606	15.6	529
14	M	67	HCC	Siemens Symbia	1.6	R	2350	4.1	916
15	M	60	HCC	Siemens Symbia	−1.0	R	3867	10.4	2262

[a]Scan gap**: the time gap between the PET/CT scan and the SPECT/CT scan; positive gap times mean that the SPECT/CT scan was performed first.
[b]R = right lobe, L = left lobe.
[c]AA: administered MS activity after correcting for decay and residual.
[d]LSF = lung shunt fraction measured by Tc-99m MAA planar imaging.
[e]mCRC = metastatic colorectal cancer.
[f]mPNET = metastatic pancreatic neuroendocrine tumor.
[g]L postoperative liver remnant.
[h]HCC = hepatocellular carcinoma.

of Y-90 imaging. A total of 7 patients were accrued in that study, but, for various technical and scheduling reasons, SPECT/CT and PET/CT data from the same patient were only available for four of those patients (patients 1–4). The second study was designed to compare dose estimates based on pretherapy Tc-99m MAA SPECT/CT and post-therapy Y-90 SPECT/CT and PET/CT imaging. The sample size to achieve these goals was 20 patients. Data from the first 11 of those patients (patients 5–15) were used for the analysis in this work as the data from the remaining nine had not yet been acquired or analyzed at the time of writing and acquisitions were performed on a different PET scanner. In both cases, patient consent was obtained to perform post-therapy Y-90 PET/CT and SPECT/CT imaging.

The two post-therapy scans were performed as close together in time as practical (all on the same day) and the order of scanning was based on scanner scheduling considerations. This paper reports results obtained for fifteen patients included in the two research protocols (mean age of 66 ± 13 yr old (y.o.); range: 43–87 y.o.; median: 63 y.o.; 11 males and 2 females, 12 right and 1 left lobar treatment). Table II gives patient demographics, information on the scanner used, and the administered activity of Y-90. Radioembolization of all patients was performed using Y-90 glass microspheres.

2.B.2. Patient image acquisition and processing

2.B.2.a. Acquisition. Each patient was imaged on one of the two SPECT/CT scanners and the PET/CT scanner. Scanner selection was based on the scanner availability considerations. The acquisition protocols and reconstruction methods were the same as for the phantom experiments. The area of the body imaged included the entire liver, if possible.

2.B.2.b. Image registration. The CT images from the SPECT and PET acquisition images were rigidly registered using the mutual information criterion using in-house software.[22] These registration parameters were then applied to the PET image to register it to the SPECT. We observed some slight residual misregistration for some patients, likely due to nonrigid deformations or respiratory motion. Nevertheless the overall registration was considered good for all patients except patients 6 and 7 based on the slice-by-slice visual examination. Most of the activities in patient 6 were concentrated in small volumes (tumors) and thus a small error in CT registration could result in a substantial difference in voxel-by-voxel activity distribution comparisons. The registration for patient 7 was difficult due to differences in patient arm position in the PET/CT and SPECT/CT studies, and significant residual misregistration was present.

2.B.2.c. VOI definition. Whole liver VOIs were manually drawn slice-by-slice using the CT images from the SPECT/CT scans. Since activity concentration in surrounding tissues was small, the VOIs were expanded by two voxels in order to account for spill-out effects.

2.B.3. Quantitative comparison and analysis

2.B.3.a. Total estimated activity. Total activities inside the liver VOI were compared. The activity in the body volume outside the liver was expected to be small for this procedure. However, in the PET images we observed nonzero voxel values outside the liver VOI. To evaluate this quantitatively, we

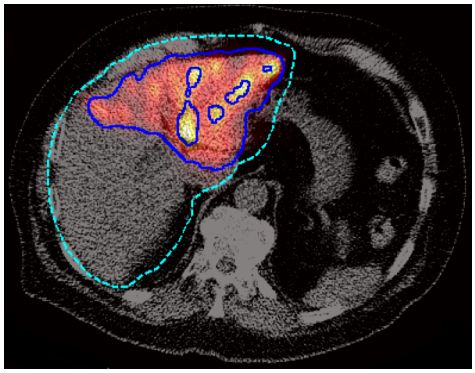

FIG. 1. Illustration of the volumes defined by the two activity concentration thresholds. A fused SPECT CT image is shown with lines indicating the boundaries of the various regions shown. The green dashed line is the liver VOI, the outer blue solid line corresponds to the boundary between the untreated and intermediate activity subvolumes, and the inner solid lines correspond to the boundary between intermediate and high activity subvolumes.

compared the ratio of the total activity inside the field-of-view and outside the liver VOI to that inside the liver VOI.

2.B.3.b. Profiles. We plotted one-pixel-wide profiles along the same line selected to cross high activity areas through the registered SPECT and PET images. The profiles compared were chosen to pass through areas of high activity in the two images.

2.B.3.c. Voxel-by-voxel correlation analysis. We generated scatter plots where the horizontal and vertical axes were the PET and SPECT voxel values, respectively. We computed the linear regression line and correlation coefficient (CC) for each patient.

2.B.3.d. Bland–Altman analysis. We used Bland–Altman plots to investigate the mean difference and standard deviation of the percent differences for each voxel. We observed a dependence of the bias and variance on the activity concentration, as discussed below. Thus the VOI volume was segmented into three subvolumes based on activity concentration thresholds: untreated subvolume (less than about 1 MBq/ml), intermediate activity subvolume (voxels in the lower 80th percentile in activity concentration among voxels outside of the previous subvolume), and high activity subvolume (the remaining upper 20th percentile of voxels). An illustration of the resulting regions is shown in Fig. 1. The mean and standard deviation of the difference in activity concentrations was calculated for each subvolume.

2.B.3.e. Activity-volume histogram. Finally, we compared the cumulative activity-volume histograms within the liver VOI for the two modalities. Histograms are not dependent on registration and are directly related to dose-volume histograms, which are potentially useful for radiobiological predictions of tumor and normal organ response.[2]

3. RESULTS

3.A. QSPECT and PET phantom experiment

Table III shows the CCFs for QSPECT and PET obtained with the various phantoms and iteration numbers. For SPECT/CT, the CCFs were different for the two systems but, for the same system, very consistent across the phantoms. The CCFs were relatively constant over the range of 5 iterations to 100 iterations. We used the average ratios from the phantom study as the calibration correction factors for the patient data. The average ratios were 0.82 for the GE and 0.86 for the Siemens systems and were used in the patient comparisons. These results indicate that QSPECT using MER, without application of the CCFs, would overestimate the true activity by 22% and 16% for the GE and Siemens scanners, respectively.

TABLE III. Phantom calibration correction factors.

	SPECT								PET
	GE Discovery				Siemens Symbia				GE Discovery
Iterations	5	10	40	100	5	10	40	100	2
Large cylinder	0.83	0.82	0.82	0.82	0.87	0.87	0.87	0.87	1.06
Small cylinder	0.83	0.82	0.81	0.81	NA				1.12
Sphere	0.83	0.83	0.83	0.83	0.85	0.85	0.85	0.85	1.17

For PET, the CCFs were phantom dependent and were greater than 1, indicating underestimation of the quantified activity. The sphere in the cold elliptical phantom had an attenuating material outside the region containing activity, and the largest discrepancy in terms of activity concentration. These differences may be due to coincidences between bremsstrahlung and annihilation photons interacting with tail extrapolation in the scatter compensation method. The average CCF over the three phantoms was ~1.12, and this was used for all the patient data presented below.

3.B. QSPECT and PET patient studies

Figure 2 shows a comparison of the Y-90 PET and SPECT images. The SPECT images here were reconstructed using the MER method; SPECT images reconstructed by standard vendor-provided algorithms had visually and quantitatively different activity distributions, as shown in Sec. 4.

3.B.1. Total liver activity

The total activities in the reconstructed images within the (whole) liver VOIs are listed in Table IV. Overall, liver activity estimates for PET and QSPECT were close. For 9 out of 15 patients, the SPECT and PET measured liver activity percentage differences were within ±5%. For 12 out of 15 patients, the differences were within ±11%. Possible reasons for the larger discrepancies in the other three cases are discussed below.

3.B.2. Extra-hepatic activity

We observed that PET reconstructed images had more apparent "activity" outside the liver VOI than SPECT reconstructed images both quantitatively and qualitatively. Y-90 activity was not expected outside the liver, except when there

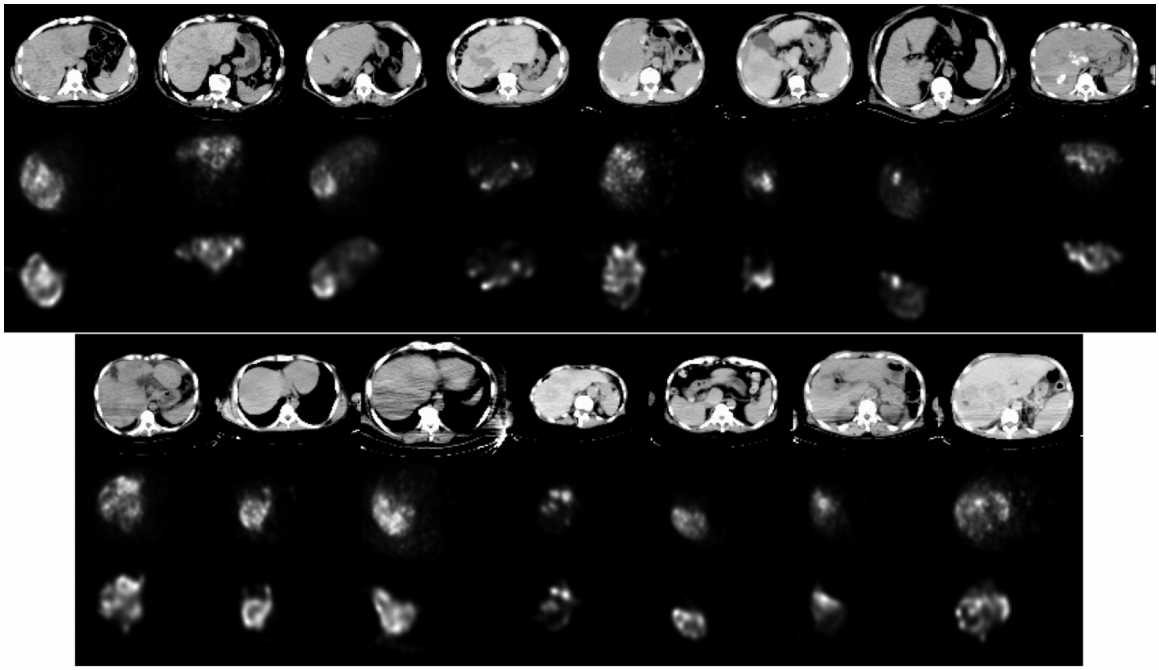

FIG. 2. CT image and activity distribution in registered PET and quantitative SPECT reconstructed images for all 15 patients. The transaxial slice with the most activity for each patient is shown. Top row: CT (from PET/CT); middle row: PET; and bottom row: quantitative SPECT. Note that corresponding PET and quantitative SPECT images are in the same gray scale.

is shunting, atypical vascular anatomy, or a less than optimal catheter placement for technical reasons. Our data suggested that Y-90 PET was inaccurate in terms of estimating activity in regions with low or no activity. Note that the activity concentration outside the liver VOI for PET was very small compared with that inside the liver, but, summed over a large volume, the total activity was non-negligible. To illustrate the magnitude of this effect, the ratio of the total activity outside the liver VOI to that of total image is shown in Table V. This ratio was much larger for PET than SPECT, even though the axial FOV for a single table position with PET/CT (~15 cm) was much smaller than for SPECT/CT (~40 cm). We observed

TABLE IV. Total activities inside liver VOI.

	PET[a] (MBq)	SPECT (MBq)	PET/injected ratio (%)	SPECT/injected ratio (%)	(SPECT-PET)/PET[b] (%)
Patient 1	3674	3601	99	97	−2
Patient 2	1678	1698	92	93	1
Patient 3	3694	3809	89	92	3
Patient 4	2564	3026	83	98	18
Patient 5	$1884^{54\%}$	2139	81	92	14
Patient 6	730	767	86	90	5
Patient 7	$3346^{93\%}$	3009	99	89	−10
Patient 8	1006	1016	92	92	1
Patient 9	$4711^{64\%}$	4726	89	89	0
Patient 10	$4504^{62\%}$	4258	94	89	−5
Patient 11	$3614^{94\%}$	2860	109	87	−21
Patient 12	1361	1447	85	91	6
Patient 13	1447	1446	90	90	0
Patient 14	1969	1975	84	84	0
Patient 15	$3688^{62\%}$	3518	95	91	−5
Mean	2658	2620	91	91	0
Std. Dev.	1304	1223	7	3	9

[a]The superscript nn% denotes cases where the PET axial FOV did not cover the whole liver. For those cases, we truncated the registered PET and SPECT images in axial direction and kept only the volume within the FOV of PET. We measured the liver activity in the truncated PET (TP), truncated SPECT (TS), and untruncated SPECT images (US). The PET activity was then estimated using $TP \times US \div TS$. The superscript nn is $TS \div US$ and was used to approximate the ratio of the liver activity in the PET FOV to that in the liver VOI.

[b]Percentage difference of activity measured by SPECT to that measured by PET.

TABLE V. Ratios of outside-VOI activity to total activity.

Patient No.	1	2	3	4	5	6	7	8	9	10	11	12	13	14	15
PET (%)	19	36	23	14	[a]	25	[a]	17	[a]	[a]	[a]	11	22	20	[a]
SPECT (%)	5	10	1	2	8	5	1	9	2	3	5	6	5	5	1

[a]The PET FOV did not cover the whole liver for these patients and was thus not included in this analysis.

the same phenomenon in phantom studies (activity outside the source volume).

3.B.3. Profiles through reconstructed images

Profiles along selected one-voxel-wide lines are shown in Fig. 3. Profiles were generated in slices from transaxial, sagittal, and coronal planes for three selected patients. For each patient, the slice with the highest total activity was selected and the profile line was drawn across the highest activity region in the slice. The profiles generally were comparable and the signal heights were similar. There were slight displacements between SPECT and PET images, likely due to residual misregistration and differences in resolution and noise properties.

3.B.4. Scatter plots

Scatter plots of the activity concentration in corresponding voxel pairs from registered QSPECT and PET reconstructed images for voxels inside the liver VOIs are shown in Fig. 4. The linear regression line and the line of identity are also shown. For patients 6 and 7, the arms were in different positions for the SPECT/CT and PET/CT scans, and so these patients were excluded from the voxel-by-voxel analyses as the images were difficult to register. Patient 11 was also excluded as an outlier because of the small scatter fraction estimated by the PET scanner software. Details are given in Sec. 4.

The slopes of the regression line were between 0.97 and 1.23 for the 12 patients. Most of the slopes were greater than and close to 1.0, while some (patients 4, 13, 14) clustered around 1.2. The correlation coefficients were between 0.86 and 0.94 for the 12 patients; all had very small (<0.01) 90% confidence intervals calculated using a bootstrap method, suggesting a strong linear relationship between voxel values for the two modalities. Taken together these data support generally excellent quantitative agreement between PET and SPECT at the voxel level.

3.B.5. Bland–Altman analysis

Bland–Altman plots of the voxels in the whole liver VOIs are shown in Fig. 5. The spread was largest when the mean was small, corresponding to regions with low activity. To investigate this more closely, we used activity thresholding to separate the liver VOI into untreated, intermediate, and high activity subvolumes, as mentioned above. Vertical lines indicate subvolume boundaries, and horizontal lines show the mean and one standard deviation values for each subvolume. The average of the percentage difference was far from zero in the untreated volumes, indicating that there was significant difference between QSPECT and PET reconstructed activity concentrations for regions with low or no activity. This analysis was consistent with the previous observation that Y-90 PET tended to overestimate the activity in very low or no activity regions, represented in Fig. 5 by the downward shifted point cloud in the untreated volumes. The threshold between untreated and intermediate activity volumes was determined for each patient so that the shifted dot cloud was within the untreated volume range. For the intermediate and high activity subvolumes, the average differences were much closer to 0. The one standard deviation lines indicate that the deviations from the mean were smaller when the mean was larger.

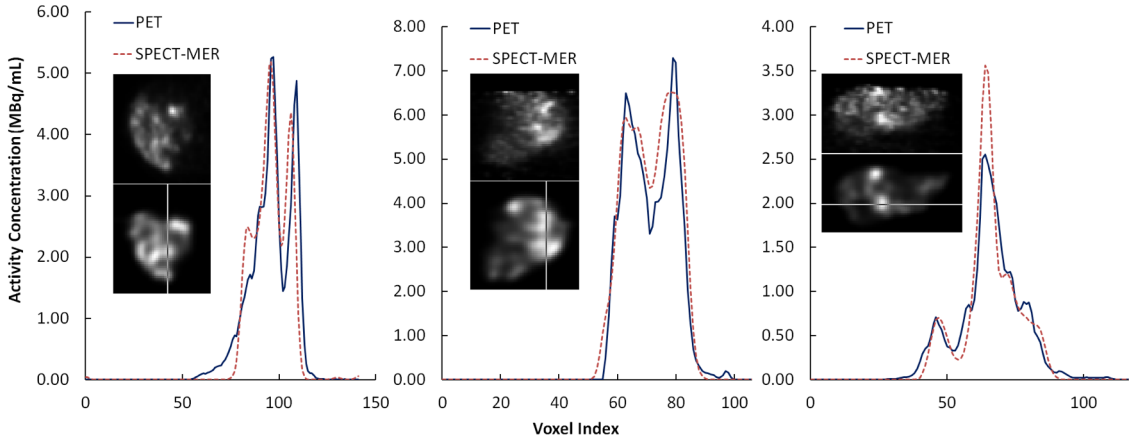

FIG. 3. Profiles through registered PET (upper) and quantitative SPECT (lower) reconstructed images along several selected one-voxel-wide lines as marked. Left: patient 1, transverse plane; middle: patient 3, coronal plane; and right: patient 4, sagittal plane.

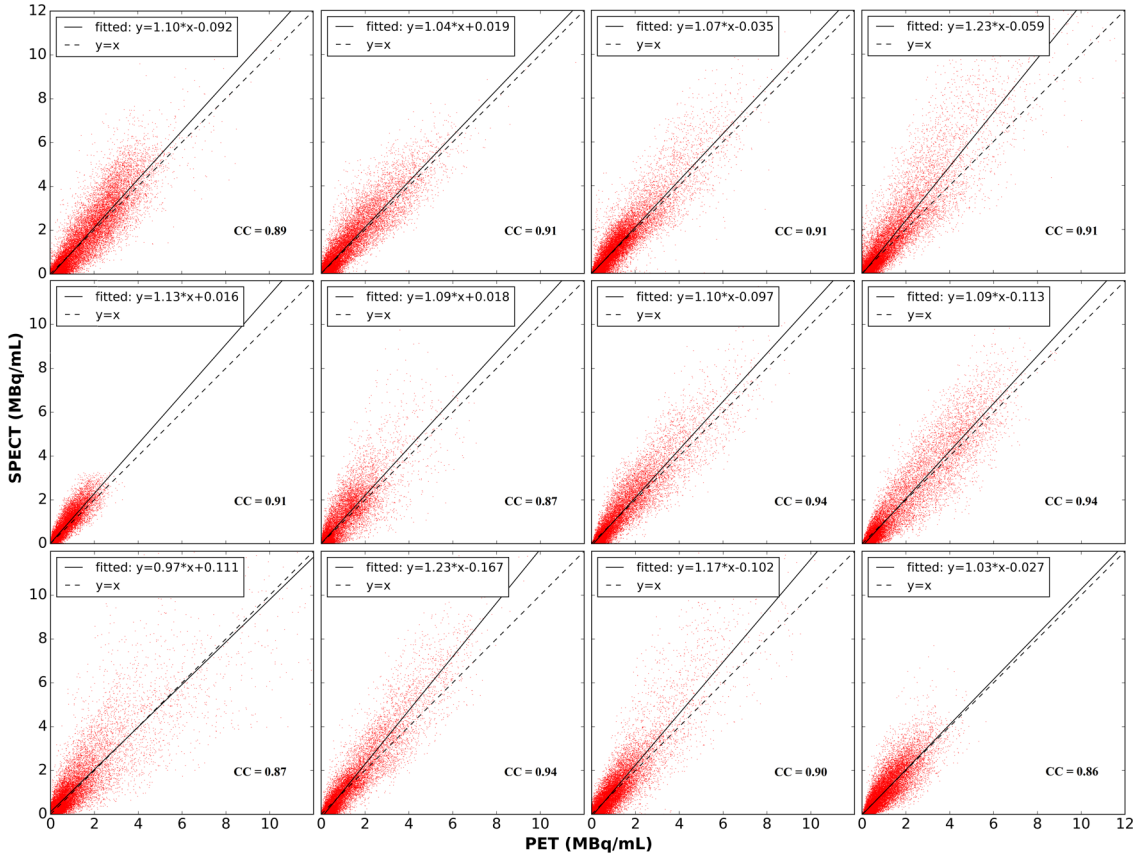

FIG. 4. Scatter plots of activity concentration in voxel pairs of registered quantitative SPECT and PET reconstructed image in liver VOIs. From left to right: top row: patients 1, 2, 3, and 4; middle row: patients 5, 8, 9, and 10; and bottom row: patients 12, 13, 14, and 15. CCs and regression line parameters are also shown.

3.B.6. Activity-volume histograms

Figure 6 shows a comparison of cumulative activity-volume histograms. The histograms indicate that PET and QSPECT provided similar estimates of the volume of the liver receiving an activity concentration higher than the value indicated on the horizontal axis. The fact that the activity-volume histograms were similar indicates that similar dose volume histograms would be obtained for both methods.

4. DISCUSSION

The phantom data in this work suggested the need for a phantom calibration rather than a rod-source sensitivity scan. A likely reason for this is incomplete knowledge of the scanner parameters and performance. However, because of its simplicity, a sensitivity measurement is likely a useful part of system quality control.

For PET, the CCFs for the different phantoms were in the range of 1.06–1.17. In Ref. 17, the accuracy for non-ToF PET with a GE scanner was −9% ±10% for the activity concentration in the background of a body-sized phantom. The CCF is defined as the ratio of the true activity divided by the measured activity. Thus, the range of estimates in Ref. 17 is consistent with the CCFs obtained in this work. It is likely that the use of ToF PET and compensation for prompt random coincidences would reduce the variation in the CCFs observed over phantoms and possibly remove the need for calibration altogether.

The data in this study indicated a good quantitative agreement between PET/CT and QBSPECT/CT using MER-based reconstruction in terms of total activity in the liver. The mean difference in total liver activity across the 15 patients was 0% ± 9%. However, three patients had a discrepancy of greater than 11%. Note that a negative discrepancy indicates that the estimate from PET was larger than from SPECT. Patient 11 had the largest negative discrepancy, −21%. For this patient, there was a physically unreasonable ratio of the liver activity estimated from PET relative to the administered activity (109%). The two patients with the largest positive difference were patients 4 (18%) and 5 (14%) and corresponded to the smallest PET/Injected activity ratios (83% and 81%), indicating that large fractions of the Y-90 was not in the liver, which is not expected. Thus, for these three cases, the PET measurements appear to be problematic.

The overestimation of PET for patient 11 might have been related to scatter undercompensation in the PET reconstruction: the scatter fraction factor (scatter counts subtracted divided by total counts) reported by the scanner was (0.17), the smallest for all the patients. Scatter undercompensation was also indicated by some high image intensities in regions, such as the arms and bed, where Y-90 is not expected. The low estimate from PET for patient 5 might be related to scatter overcompensation, since the scatter fraction factor

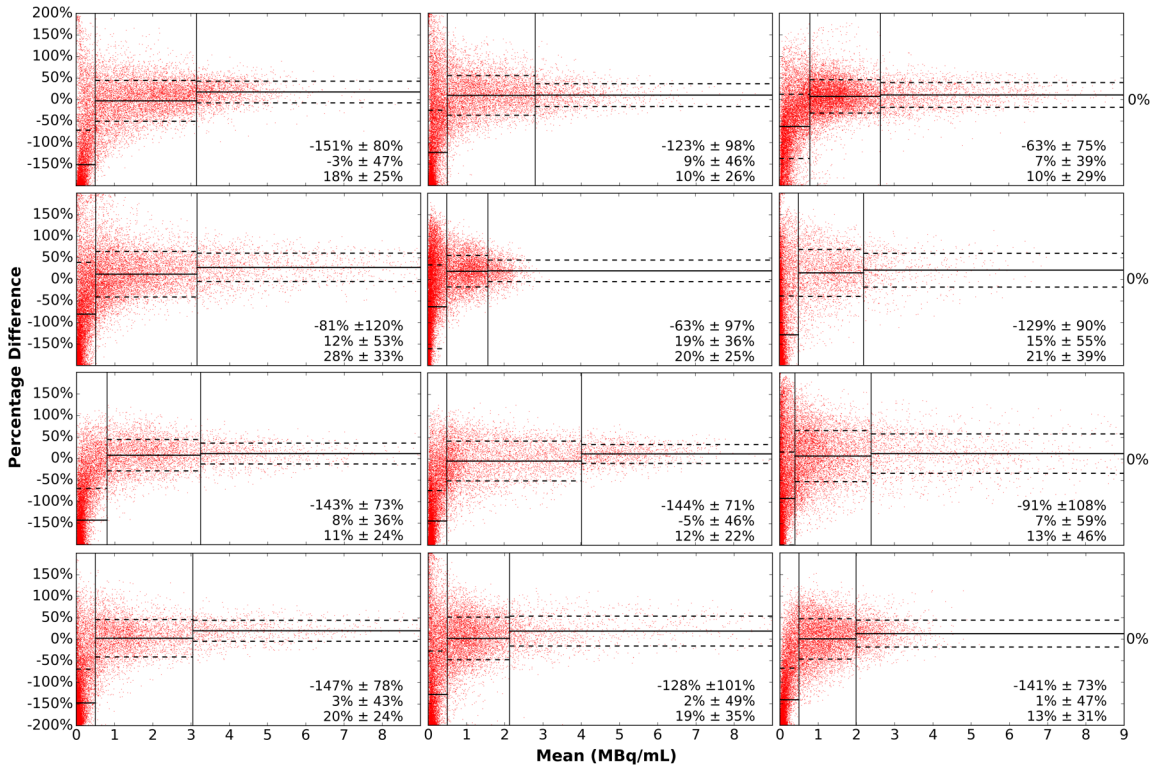

FIG. 5. Bland–Altman plots with mean and percentage difference between the Y-90 SPECT and PET voxel values plotted on the horizontal and vertical axes, respectively. Lines indicating the average difference (solid) and one standard deviation (1 std) line (dashed) are drawn for the three activity concentration ranges. The mean ±1 std value of three ranges is listed at the right bottom corner. Top row: patients 1, 2, and 3; second row: patients 4, 5, and 8; third row: patients 9, 10, and 12; and bottom row: patients 13, 14, and 15.

was the largest (0.49) among all patients. The scatter fraction factors for the other patients were between 0.19 and 0.40. The largest two negative total liver activity differences (patient 11, −21% and patient 7, −11%) corresponded to patients with the largest body cross sectional areas (torso slice area: 1031 and 1113 cm^2), while the sizes for the other patients ranged from 417 to 859 cm^2. The torso size differences are illustrated in Fig. 2. This suggests that PET accuracy might be a function of body size, consistent with the PET calibration phantom results.

The large positive discrepancy of 18% for patient 4 did not seem related to scatter compensation or patient size. One possible source of difference is that there was a relatively high activity concentration near the border of the PET FOV. Also, both the PET and SPECT images indicated an activity distribution that was dominated by relatively small areas of focal uptake (refer to Fig. 3, right). Activity for other patients was more uniformly distributed (e.g., refer to Fig. 3, left and middle). Based on the data from phantom experiments, the CCF for Y-90 PET was object- and concentration-dependent. Thus, one possible explanation of the larger difference for patient 4 is that the CCF used was for an activity distribution quite different from that seen in patient 4.

As mentioned in Sec. 3, we observed in both phantom studies and patient studies that non-ToF PET tended to overestimate activity in regions with low or no activity. Others have also reported this phenomenon.[17,23] One possible explanation is a "prompt coincidence" between a bremsstrahlung photon and an annihilation photon, similar to the case of I-124 and Y-86.[24,25] Since these events do not result from random coincidences, they would not be compensated for by a randoms correction. The distribution of these photons is expected to be broad and could extend outside the body. This could result in interaction with extrapolation of scatter tails outside the body and give rise to incorrect scatter compensation and a resulting loss of accuracy. The effect would be largest in regions with low or no activity. In addition, pair production created by high-energy bremsstrahlung photons in LYSO crystals is possible. This will generate additional signal and affect reconstruction accuracy.[26] It is quite likely that the use of ToF PET and prompt coincidence compensation methods would reduce the variability of the CCFs seen in phantoms and improve the accuracy of PET activity estimates.[17]

The largest deviations in regression line slope from unity were observed for patients 4, 13, and 14, where the slope was about 1.2. A slope value larger than one means that SPECT gave larger estimates of the voxel values than PET. The large slope for patient 4 corresponds to the greatest positive difference in total activity estimation as shown in Table IV. However, the total organ activity differences for patients 13 and 14 were still close to 0, even though there was a large difference in total activity, because the slope is more strongly influenced by voxels with higher activity concentrations, and relative overestimation of SPECT in high activity voxels cancelled out relative overestimation of PET in low activities voxels.

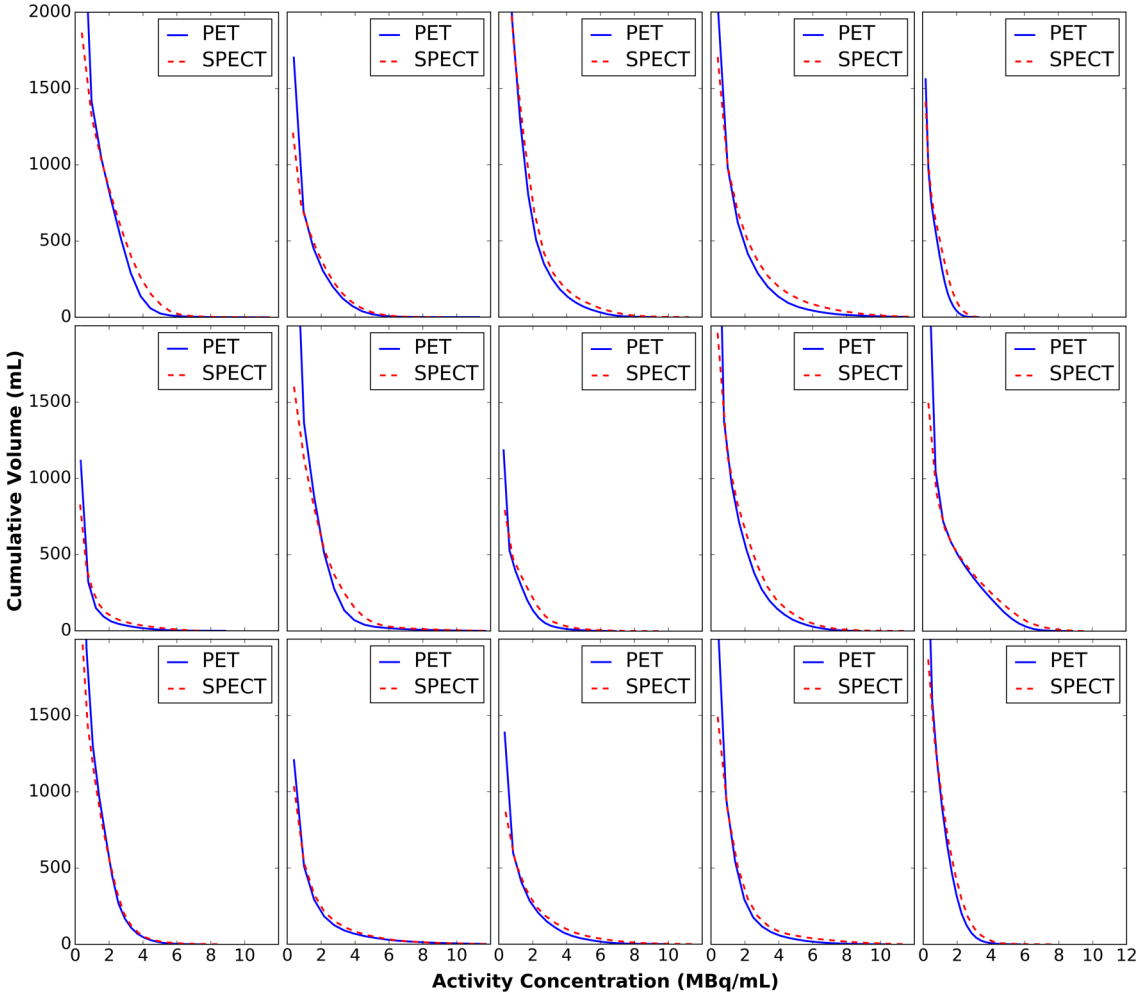

FIG. 6. Cumulative activity-volume histograms for PET and QSPECT images. Top row: patients 1, 2, 3, 4, and 5; middle row: patients 6, 7, 8, 9, and 10; and bottom row: patients 11, 12, 13, 14, and 15.

The Bland–Altman plots further demonstrate the good agreement between the modalities. The mean difference was largest in the regions with very low activities, corresponding to the untreated volume of the liver. The mean differences were smaller in intermediate or high activity subvolumes. This is consistent with the observation that the PET/CT imaging method used in this work tended to overestimate activity concentrations in regions of low activity for Y-90.

One explanation for the variation in differences for a given mean activity concentration being larger for lower activities is image noise. For images reconstructed with OS-EM, the variance is proportional to the mean.[27–29] If the discrepancy is dominated by noise, then we would expect the standard deviation of the difference in voxel values for the two modalities to be proportional to the square root of the mean. Figure 7 plots the difference over the square root of the mean versus the mean for each voxel. If the difference was due only to noise, this curve should be a horizontal line. In addition, we calculated the mean and standard deviation of the difference divided by the square root of the mean in 20 intervals evenly divided over the range of mean voxel values. Note that the standard deviations for these ranges were relatively constant, indicating that the variations about the mean were largely due to noise. Deviations from the horizontal line and constant standard deviations occurred in regions of low activity concentration, consistent with previous observations. As also observed previously, the mean difference was close to zero and relatively constant over much of the range of activities.

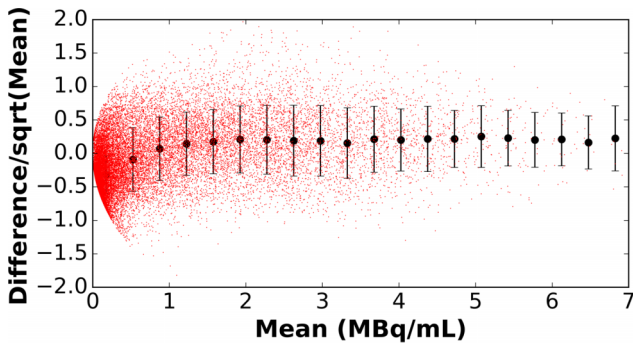

FIG. 7. Standard deviations of the difference between PET and SPECT for patient 2 divided by the square root of the mean drawn for intervals spanning equal ranges of activity concentration.

5. CONCLUSIONS

In this work, we compared quantitative Y-90 bremsstrahlung SPECT images reconstructed using the previously developed MER-based method and Y-90 PET images reconstructed by OSEM without ToF or resolution recovery. We measured a calibration correction factor for the SPECT images obtained from extended sources for both a GE Discovery 670 and a Siemens Symbia T16. This factor was found to be relatively independent of the object shape and activity distribution. For Y-90 PET using a GE Discovery RX PET/CT system without ToF or prompt coincidence correction capabilities, a phantom calibration was also needed, but the calibration correction factor was object-dependent. We compared both the total activity in the liver and the voxel-by-voxel activity distribution in 15 patients imaged with both Y-90 PET/CT and SPECT/CT. The data indicated that the PET images from this scanner overestimated the Y-90 activity concentration in regions with low or no activity. Voxel-by-voxel comparisons showed good agreement in regions corresponding roughly to treated normal liver and tumor. The magnitudes of deviations in regions of higher activity were consistent with deviations due to image noise. Cumulative activity-volume histograms were also in good agreement, indicating that the modalities would produce comparable results in terms of relative 3D dosimetric quantities. The results of this study indicate that Y-90 SPECT/CT with appropriate reconstruction methods and Y-90 PET/CT are comparable in terms of estimating total activity in the liver and activity distributions within treated volumes. Thus the choice of these two methods can be based on other considerations such as practicality and size of the FOV. For the scanner used, the PET activity distribution in regions with low or zero uptake appeared to be overestimated. In conclusion, both modalities are suitable for post-therapy monitoring of intrahepatic Y-90 activity distribution following radioembolization.

ACKNOWLEDGMENTS

This work was partially supported by BTG Interventional Medicine, the manufacturer of TheraSphere. This work was also partially supported by the National Cancer Institute of the National Institutes of Health Public Health Service Grant Nos. R01-CA109234 and U01-CA140204. The content is solely the responsibility of the authors and does not necessarily represent the official views of the National Institutes of Health.

CONFLICT OF INTEREST DISCLOSURE

Portions of the software used to reconstruct the Tc-99m and Y-90 images have been licensed to GE Healthcare by Johns Hopkins University. One of the authors, E. C. Frey, receives a portion of the licensing revenue. The terms of this arrangement are being managed by the Johns Hopkins University in accordance with its conflict of interest policies.

[a]Author to whom correspondence should be addressed. Electronic mail: efrey@jhmi.edu; Telephone: 443-287-2426.

[1]W. A. Dezarn, J. T. Cessna, L. A. DeWerd, W. Feng, V. L. Gates, J. Halama, A. S. Kennedy, S. Nag, M. Sarfaraz, V. Sehgal, R. Selwyn, M. G. Stabin, B. R. Thomadsen, L. E. Williams, and R. Salem, "Recommendations of the American Association of Physicists in Medicine on dosimetry, imaging, and quality assurance procedures for ^{90}Y microsphere brachytherapy in the treatment of hepatic malignancies," Med. Phys. **38**, 4824–4845 (2011).

[2]K. S. Kolbert, G. Sgouros, A. M. Scott, J. E. Bronstein, R. A. Malane, J. Zhang, H. Kalaigian, S. McNamara, L. Schwartz, and S. M. Larson, "Implementation and evaluation of patient-specific three-dimensional internal dosimetry," J. Nucl. Med. **38**, 301–308 (1997).

[3]A. K. Jha, A. A. Zade, V. Rangarajan, N. Purandare, S. A. Shah, A. Agrawal, S. S. Kulkarni, and N. Shetty, "Comparative analysis of hepatopulmonary shunt obtained from pretherapy ^{99m}Tc MAA scintigraphy and post-therapy ^{90}Y bremsstrahlung imaging in ^{90}Y microsphere therapy," Nucl. Med. Commun. **33**, 486–490 (2012).

[4]H. A. Ziessman, R. L. Wahl, J. E. Juni, J. E. Gyves, W. D. Ensminger, J. H. Thrall, J. W. Keyes, Jr., and S. C. Walker, "The utility of SPECT for ^{99m}Tc-MAA hepatic arterial perfusion scintigraphy," Am. J. Roentgenol. **145**, 747–751 (1985).

[5]E. Garin, L. Lenoir, Y. Rolland, J. Edeline, H. Mesbah, S. Laffont, P. Poree, B. Clement, J. L. Raoul, and E. Boucher, "Dosimetry based on ^{99m}Tc-macroaggregated albumin SPECT/CT accurately predicts tumor response and survival in hepatocellular carcinoma patients treated with ^{90}Y-loaded glass microspheres: Preliminary results," J. Nucl. Med. **53**, 255–263 (2012).

[6]H. Ahmadzadehfar, A. Sabet, K. Biermann, M. Muckle, H. Brockmann, C. Kuhl, K. Wilhelm, H. J. Biersack, and S. Ezziddin, "The significance of ^{99m}Tc-MAA SPECT/CT liver perfusion imaging in treatment planning for ^{90}Y-microsphere selective internal radiation treatment," J. Nucl. Med. **51**, 1206–1212 (2010).

[7]E. Garin, L. Lenoir, Y. Rolland, S. Laffont, M. Pracht, H. Mesbah, P. Poree, V. Ardisson, P. Bourguet, B. Clement, and E. Boucher, "Effectiveness of quantitative MAA SPECT/CT for the definition of vascularized hepatic volume and dosimetric approach: Phantom validation and clinical preliminary results in patients with complex hepatic vascularization treated with yttrium-90-labeled microspheres," Nucl. Med. Commun. **32**, 1245–1255 (2011).

[8]M. Wondergem, M. L. Smits, M. Elschot, H. W. de Jong, H. M. Verkooijen, M. A. van den Bosch, J. F. Nijsen, and M. G. Lam, "^{99m}Tc-macroaggregated albumin poorly predicts the intrahepatic distribution of ^{90}Y resin microspheres in hepatic radioembolization," J. Nucl. Med. **54**, 1294–1301 (2013).

[9]M. Elschot, M. G. Lam, M. A. van den Bosch, M. A. Viergever, and H. W. de Jong, "Quantitative Monte Carlo-based ^{90}Y SPECT reconstruction," J. Nucl. Med. **54**, 1557–1563 (2013).

[10]D. Minarik, K. Sjogreen-Gleisner, O. Linden, K. Wingardh, J. Tennvall, S. E. Strand, and M. Ljungberg, "^{90}Y Bremsstrahlung imaging for absorbed-dose assessment in high-dose radioimmunotherapy," J. Nucl. Med. **51**, 1974–1978 (2010).

[11]X. Rong, Y. Du, M. Ljungberg, E. Rault, S. Vandenberghe, and E. C. Frey, "Development and evaluation of an improved quantitative ^{90}Y bremsstrahlung SPECT method," Med. Phys. **39**, 2346–2358 (2012).

[12]E. Rault, E. Clementel, S. Vandenberghe, Y. D'Asseler, R. Van Holen, J. De Beenhouwer, and S. Staelens, "Comparison of yttrium-90 SPECT and PET images," J. Nucl. Med. **51**, 125 (2010).

[13]M. Elschot, B. J. Vermolen, M. G. E. H. Lam, B. de Keizer, M. A. A. J. van den Bosch, and H. W. A. M. de Jong, "Quantitative comparison of PET and bremsstrahlung SPECT for imaging the *in vivo* yttrium-90 microsphere distribution after liver radioembolization," PLoS One **8**, e55742 (2013).

[14]V. L. Gates, A. A. Esmail, K. Marshall, S. Spies, and R. Salem, "Internal pair production of ^{90}Y permits hepatic localization of microspheres using routine PET: Proof of concept," J. Nucl. Med. **52**, 72–76 (2011).

[15]Y. H. Kao, E. H. Tan, K. Y. Lim, C. E. Ng, and S. W. Goh, "Yttrium-90 internal pair production imaging using first generation PET/CT provides high resolution images for qualitative diagnostic purposes," Br. J. Radiol. **85**, 1018–1019 (2011).

[16]R. Lhommel, P. Goffette, M. Van den Eynde, F. Jamar, S. Pauwels, J. I. Bilbao, and S. Walrand, "Yttrium-90 TOF PET scan demonstrates high-resolution biodistribution after liver SIRT," Eur. J. Nucl. Med. Mol. Imaging **36**, 1696 (2009).

[17]K. P. Willowson, M. Tapner, and D. L. Bailey, "A multicentre comparison of quantitative ^{90}Y PET/CT for dosimetric purposes after radioembolization with resin microspheres," Eur. J. Nucl. Med. Mol. Imaging **42**, 1202–1222 (2015).

[18]Y. Du, B. M. W. Tsui, and E. C. Frey, "Model-based compensation for quantitative I-123 brain SPECT imaging," Phys. Med. Biol. **51**, 1269–1282 (2006).
[19]D. Minarik, K. Sjogreen Gleisner, and M. Ljungberg, "Evaluation of quantitative ^{90}Y SPECT based on experimental phantom studies," Phys. Med. Biol. **53**, 5689–5703 (2008).
[20]B. E. Zimmerman, J. T. Cessna, and M. A. Millican, "Experimental determination of calibration settings for plastic syringes containing solutions of ^{90}Y using commercial radionuclide calibrators," Appl. Radiat. Isot. : including data, instrumentation and methods for use in agriculture, industry and medicine **60**, 511–517 (2004).
[21]E. C. Frey and B. M. W. Tsui, *presented at The Nuclear Science Symposium and Medical Imaging Conference*, 1996 (unpublished).
[22]P. Viola and W. M. Wells III, *presented at The Computer Vision Proceedings of Fifth International Conference*, 1995 (unpublished).
[23]K. N. Tapp, W. B. Lea, M. S. Johnson, M. Tann, J. W. Fletcher, and G. D. Hutchins, "The impact of image reconstruction bias on PET/CT ^{90}Y dosimetry after radioembolization," J. Nucl. Med. **55**, 1452–1458 (2014).
[24]H. Herzog, L. Tellmann, B. Scholten, H. H. Coenen, and S. M. Qaim, "PET imaging problems with the non-standard positron emitters yttrium-86 and iodine-124," Q. J. Nucl. Med. Mol. Imaging **52**, 159–165 (2008).
[25]S. Walrand, F. Jamar, I. Mathieu, J. De Camps, M. Lonneux, M. Sibomana, D. Labar, C. Michel, and S. Pauwels, "Quantitation in PET using isotopes emitting prompt single gammas: Application to yttrium-86," Eur. J. Nucl. Med. Mol. Imaging **30**, 354–361 (2003).
[26]L. van Elmbt, S. Vandenberghe, S. Walrand, S. Pauwels, and F. Jamar, "Comparison of yttrium-90 quantitative imaging by TOF and non-TOF PET in a phantom of liver selective internal radiotherapy," Phys. Med. Biol. **56**, 6759–6777 (2011).
[27]E. J. Soares, C. L. Byrne, and S. J. Glick, "Noise characterization of block-iterative reconstruction algorithms: I. Theory," IEEE Trans. Med. Imaging **19**, 261–270 (2000).
[28]H. H. Barrett, D. W. Wilson, and B. M. W. Tsui, "Noise properties of the EM algorithm. I. Theory," Phys. Med. Biol. **39**, 833–846 (1994).
[29]D. W. Wilson, B. M. W. Tsui, and H. H. Barrett, "Noise properties of the EM algorithm. II Monte Carlo simulations," Phys. Med. Biol. **39**, 847–871 (1994).